Graphene and 2D Materials
https://doi.org/10.1007/s41127-024-00083-9

REVIEW ARTICLE

Functionality review and life cycle assessment of a silver-based MOF for advanced material and sustainability applications

Mostafa Dadashi Firouzjaei[1] · Ahmad Arabi Shamsabadi[2] · Ahmad Rahimpour[3] · Farhad Akbari Afkhami[4] · Mark Elliott[1]

Received: 9 August 2024 / Revised: 29 September 2024 / Accepted: 2 November 2024

Abstract
This review provides an in-depth analysis of the synthesis, properties, and diverse applications of silver-based metal–organic frameworks (U-AgMOFs), with a focus on those synthesized via ultrasonication. The term "U-AgMOF" is used to reflect the use of ultrasonication in its fabrication, which allows for precise control over its nanoscale structure. U-AgMOF exhibits enhanced antibacterial properties and strong compatibility with two-dimensional materials like graphene oxide and $Ti_3C_2T_x$ MXene. U-AgMOFs show significant promise in applications such as antibacterial coatings, membrane technologies, and environmental remediation. Key findings include 98% methylene blue dye adsorption efficiency, a 75% reduction in *Escherichia coli* growth at a concentration of 100 µg/mL and a 25% improvement in water permeability when incorporated into thin-film nanocomposite membranes. U-AgMOFs have also demonstrated over 80% apoptosis induction in colon cancer cells at 200 µg/mL. Additionally, this review presents the first life cycle assessment of any MOF, offering insights into its environmental impact and energy consumption, with recommendations for improving sustainability in future production.

Keywords Silver · Metal–organic framework (MOF) · Hybrid composites · Functional properties · Life cycle assessment (LCA) · Separation

1 Introduction to the metal–organic frameworks (MOFs)

The concept of metal–organic frameworks (MOFs) has evolved significantly since its early mentions in the mid-twentieth century. In 1965, materials that would today be classified as MOFs were initially referenced [1]. These early forms of MOFs were composed of bi- and trivalent aromatic carboxylic acids that formed frameworks with various metals, including zinc, nickel, iron, aluminum, thorium, and uranium. Even at this nascent stage, notable properties like high thermal stability and significant metal content were observed [2]. This period also observed reports on crystalline polymeric compounds, such as Cu(II) tricyanomethanide, which can be retrospectively recognized as part of the MOF family [3]. The field of MOFs gained renewed attention in the 1990s, particularly with the works of Hoskins and Robson, who reported on scaffold-like materials using Cu(I) centers [4]. A significant milestone was achieved by the group of Yaghi in 1999, which introduced the concept of reticular design, marking a new era in MOF research [5].

Yaghi's group successfully synthesized MOF-5, demonstrating exceptional stability and high porosity [5]. This MOF is synthesized using a dicarboxylate linker that, when combined with metal carboxylates like Zn^{2+}, forms a distinct oxide-centered tetranuclear supertetrahedral cluster (Fig. 1). These clusters are interconnected to create a three-dimensional (3D) framework with a significantly higher surface area and pore volume than most crystalline zeolites. The synthesis is carried out by

✉ Mostafa Dadashi Firouzjaei
mdfirouzjaei@crimson.ua.edu

✉ Mark Elliott
melliott@eng.ua.edu

[1] Department of Civil, Construction, and Environmental Engineering, University of Alabama, Tuscaloosa, AL 35487, USA

[2] Department of Chemistry, University of Pennsylvania, Philadelphia, PA 19104, USA

[3] Flexim Manufacturing Services Incorporation, Edmonton, AB, Canada

[4] Department of Chemistry, University of Alabama, Tuscaloosa, AL 35487, USA

Published online: 09 November 2024

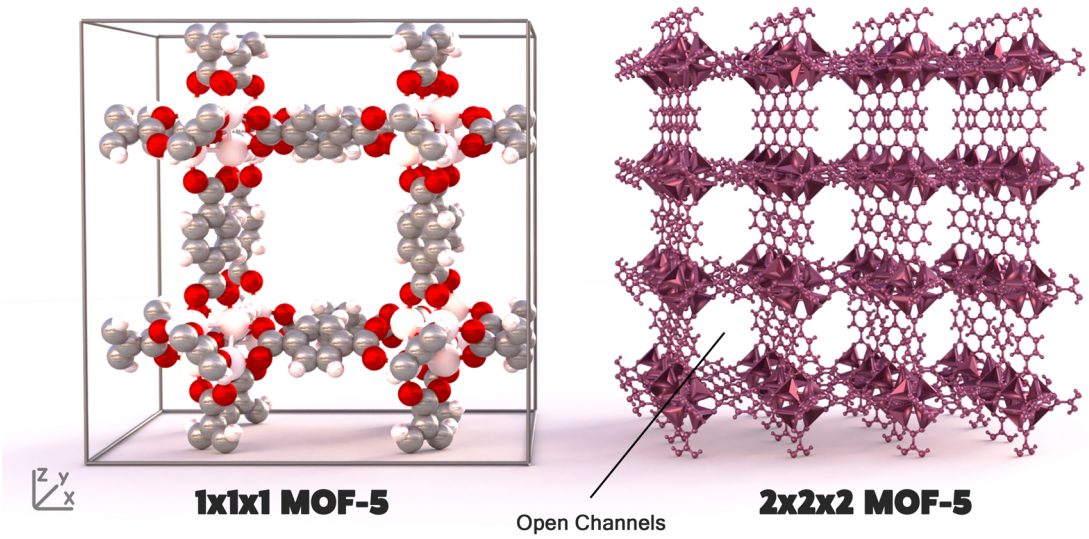

Fig. 1 Comparative visualization of the 1×1×1 and 2×2×2 unit cell configurations of MOF-5, illustrating the oxide-centered tetranuclear clusters (represented in the 1×1×1 model) and the resultant augmented 3D framework (demonstrated in the 2×2×2 model)

diffusing triethylamine into a solution of zinc (II) nitrate and H_2BDC in dimethylformamide/chlorobenzene, leading to the formation of colorless cubic crystals of MOF-5. The stability of MOF-5 is remarkable, maintaining its crystallinity and structure even when fully desolvated and heated up to 300 °C. X-ray single-crystal diffraction studies confirm the expected topology of the framework, and gas sorption isotherms reveal a reversible type I isotherm, indicating uniform pores with an estimated Langmuir surface area of 2900 m2/g. This MOF's stability, even in the absence of guest molecules, and its high surface area make it a promising candidate for various applications in catalysis, gas storage, and molecular recognition.

MOFs manifest a distinct divergence from traditional solid-state materials such as zeolites, carbons, and oxides, primarily attributable to their exceptional framework pliability [5]. This inherent flexibility facilitates MOFs to undergo conformational modifications, including contraction or dilation, contingent upon the presence or absence of guest molecules [6]. This characteristic adaptability is conspicuously absent in more structurally rigid frameworks exemplified by zeolites or carbon-based materials. A salient attribute of MOFs is their elimination of non-accessible bulk volume, frequently denominated as "dead volume [7]." In conventional porous materials, a fraction of the internal volume remains inaccessible for molecular adsorption or interaction, thereby constraining their functional efficacy in scenarios necessitating elevated surface area and porosity [8]. Conversely, MOFs are engineered to optimize accessibility, thereby enabling the entirety of their internal volume to be utilized for molecular interaction. This feature substantially augments their functional efficiency in myriad applications, such as gas storage, where maximal surface area exposure is of paramount importance [9, 10].

The synthesis of MOFs is a remarkably streamlined and versatile process, which has contributed to the rapid growth and diversity of the MOF family. This process is considered simple because it involves straightforward steps, including the use of well-soluble metal salts such as nitrates, sulfates, or acetates [11], combined with organic components like mono-, di-, tri-, and tetracarboxylic acids [12]. These components are typically introduced into a polar organic solvent, such as an amine or amide like triethylamine, diethylformamide, or dimethylformamide [12]. Within this mixture, the metal ions and organic ligands self-assemble into highly ordered structures, enabling the creation of complex and highly regular frameworks without the need for intricate fabrication techniques [13]. This self-assembly is a hallmark of MOF synthesis. Temperature flexibility also plays a crucial role, with synthesis possible under a range of conditions, from ambient room temperature to solvothermal processes reaching up to 200 °C [14]. This flexibility allows for customization of MOF properties, including control over the size, shape, and porosity of the resulting framework [15], making it suitable for a broad range of applications.

Certain MOFs have attracted considerable interest in the vast array of synthesized MOFs due to their notable surface properties and effectiveness in various applications. MOF-177 is distinguished by its exceptional surface area, which is quantified at 5640 m2/g [16]. This parameter is critical for hydrogen storage, where MOF-177 can adsorb up to 7.5 wt% hydrogen at 77 K and pressures reaching 70 bar [17]. MIL-101, with a recorded surface area nearing 5870 m^2/g and pore volumes as high as 1.85 cm^3/g, excels

in applications necessitating vast gas adsorption capacities [18]. With an average pore diameter of over 2.9 nm and a capacity to withstand high temperatures of up to 300 °C, this material is highly suitable for absorbing heavy metals such as lead. It can achieve a removal efficiency of over 99% [19]. HKUST-1, with its active copper centers, is tailored for catalytic functions [20]. For example, pretreatment of the HKUST-1 catalyst with water significantly accelerated its catalytic activity in the oxidation of benzene, with a turnover frequency (TOF) of 35.1 h^{-1}, demonstrating its adaptability and enhanced efficiency in catalytic reactions [21]. The recovery and recyclability of HKUST-1 have been demonstrated, with minimal loss of activity after several cycles of use [22]. ZIF-8's thermal endurance, up to 550 K, and its chemical inertness under aggressive conditions make it suitable for gas separation, particularly in CO_2 capture, where it demonstrates a CO_2/N_2 selectivity of 30.0 at 298 K [23]. The interaction energy between CO_2 and the Zn–N bonds in ZIF-8 is estimated at − 15.1 kcal/mol, facilitating selective adsorption [24]. UiO-66 exhibits remarkable zirconium-based framework stability, maintaining its structure post-exposure to pH ranges between 1 and 12 [25]. In drug delivery, UiO-66 has been shown to encapsulate ibuprofen, with a loading of approximately 0.6 g/g, and sustain its release over 400 min. The structural adaptability of UiO-66, combined with its biocompatibility, presents a versatile platform for the targeted and controlled release of therapeutic agents [25]. Figure 2 illustrates some of the most studied MOFs.

2 Study objectives

The manuscript aims to offer a comprehensive assessment of a multifunctional silver-based metal–organic framework (U-AgMOF) fabricated by our research team in 2018 [26]. To differentiate this U-AgMOF from other reported AgMOFs, we labeled it U-AgMOF (the letter "U" is from the ultrasonic) in the remaining parts of this manuscript. This U-AgMOF has been strategically utilized in various fields, such as antibacterial nanomaterials, water treatment, cancer research, and anti-biofouling surfaces, due to its unique synthesis and properties, demonstrating its broad effectiveness and versatility. This work is distinguished by incorporating a life cycle assessment (LCA), a novel approach for this specific MOF, that reveals the environmental impact from the beginning to the end of its lifecycle. The addition of an LCA analysis sets our paper apart from other reviews on MOFs. It enhances a thorough comprehension of the environmental impacts of U-AgMOF, paving the way for the establishment of sustainable practices in material science. Other sections delve into the diverse applications of U-AgMOF, analyzing its synergistic interactions with GO and MXenes, its flexible synthesis methods, and the resulting environmental and health impacts with a short review of the industrial status of MOFs.

3 Synthesis and unique characteristic features of U-AgMOF

The method used to synthesize the U-AgMOF involves utilizing sonochemistry, which uses acoustic cavitation to create localized high-temperature and high-pressure areas, followed by quick cooling. This creates a favorable setting for the development of nanoscale materials. For the U-AgMOF, the reaction conditions involve 0.5 g of benzene-1,3,5-tricarboxylic acid (BTC) in 20 mL of ethanol and an equal mass of silver nitrate in 20 mL of deionized water to achieve a 1:1 stoichiometric ratio, which is essential for the desired coordination geometry around the silver centers. Ethanol was chosen as a solvent for BTC due to its lower dielectric constant compared to water, which enables a higher level of

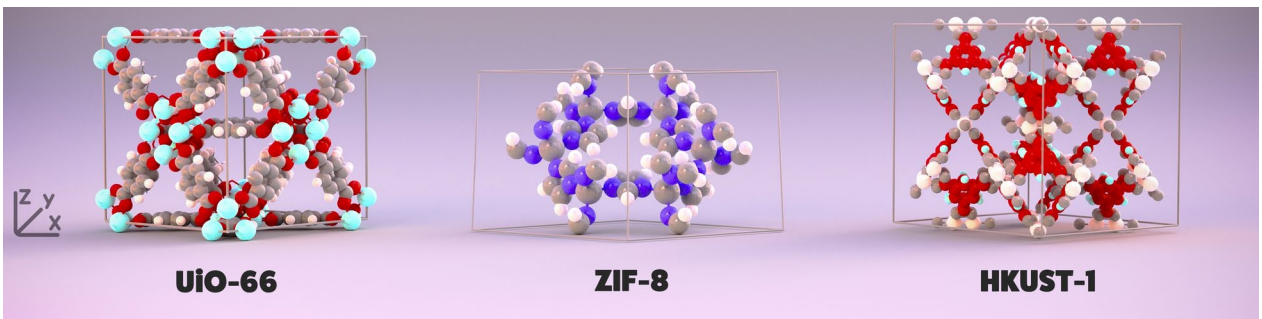

Fig. 2 Representative structures of UiO-66, ZIF-8, and HKUST-1 MOFs, showcasing their distinct lattice frameworks. UiO-66 is depicted with its zirconium-based nodes and organic linkers, demonstrating the stability that facilitates its use in pH-sensitive applications like drug delivery. ZIF-8, with its characteristic sodalite topology, illustrates the thermal and chemical resilience pertinent to CO_2/N_2 gas separation. HKUST-1 is visualized with its copper centers, highlighting the active sites responsible for its catalytic efficiency and the capacity for benzene oxidation with significant turnover frequency. These frameworks exemplify the structural diversity and functional adaptability that underpin the wide-ranging applications of MOFs in gas storage, separation, catalysis, and biomedicine

ligand deprotonation and coordination with the silver ion. Moreover, ethanol's volatility plays a key role in eliminating solvent molecules in the post-synthesis drying process, which is crucial for achieving solvent-free MOF structures.

Figure 3a shows the schematic fabrication process of U-AgMOF. The ultrasonic irradiation parameters of 20 kHz frequency, 100 watts output energy, and a 0.6 pulse duration are fine-tuned to stimulate the creation of metal–organic linkages via cavitation. The ultrasonic energy input is used to break intermolecular forces in the solvent, which increases the solubility of reactants and helps create a more uniform reaction mixture. Optimal energy and pulse parameters are crucial. Excessive energy could result in uncontrolled growth or disintegration of the MOF lattice, whereas inadequate energy may not provide the required activation for MOF assembly. After being exposed to radiation, the

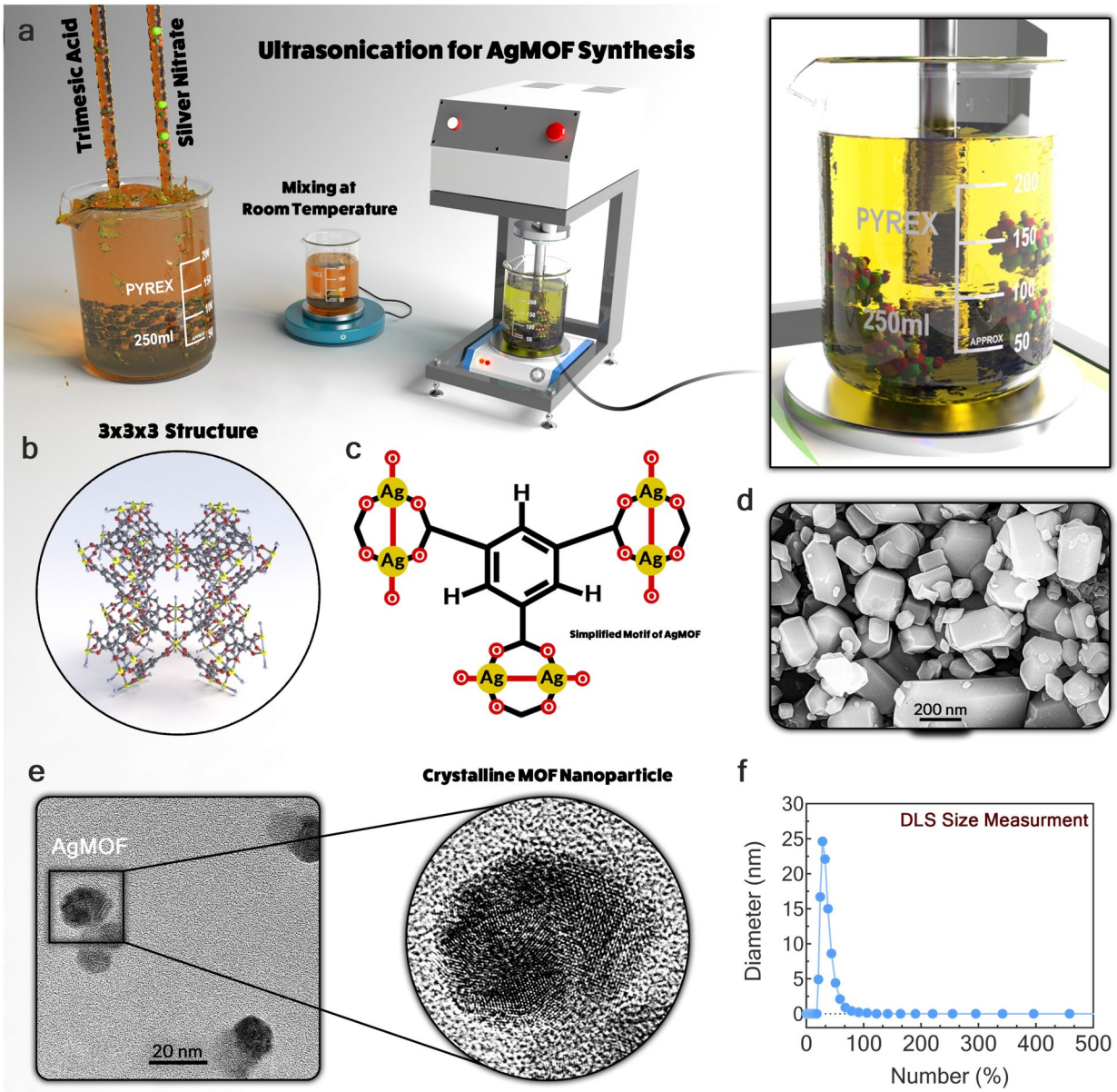

Fig. 3 The multifaceted process and structural insights into U-AgMOF synthesis via ultrasonication highlight its stoichiometric chemical orchestration and the resulting morphological characteristics. **a** The sonochemical setup yields a homogeneous reaction mixture for U-AgMOF production. **b** The 3D structural framework of U-AgMOF, demonstrating the complex coordination geometry around silver ions, and **c** The simplified chemical structure of U-AgMOF. **d** SEM image of the U-AgMOF, **e** TEM image of U-AgMOF, **f** the DLS size distribution, emphasizing the consistency in nanoparticle size crucial for their stability and applicability in various industrial domains. This figure encapsulates the comprehensive approach from chemical reaction to analyzing the synthesized MOF's physical properties

MOF structures come together and crystallize, resulting in the creation of white precipitates. The color change is likely due to the d–d transitions occurring within the silver coordination complexes, indicating the successful assembly of the MOF. The drying process involves maintaining a controlled temperature of 35 °C for 24 h to preserve the U-AgMOF structure. The selected temperature is higher than room temperature to speed up solvent evaporation but significantly lower than the level that could cause thermal degradation of the metal–ligand bonds or structural collapse due to rapid solvent evaporation [27]. This step is crucial for maintaining the mesoporosity and crystallinity of the U-AgMOF, which are necessary for its future use in different applications.

Figure 3b–c shows the 3D and simplified chemical structure of the U-AgMOF. The X-ray photoelectron spectroscopy (XPS) and Fourier-transform infrared (FT-IR) spectroscopy results offer in-depth information about the chemical composition of the U-AgMOF. The XPS analysis of the U-AgMOF spectra shows the presence of carbon (C 1s) and oxygen (O 1s) elements, along with silver (Ag 3d) [26]. The U-AgMOF showed a high concentration of silver, indicated by the prominent Ag 3d peaks at around 368.2 eV for Ag $3d_{5/2}$ and 374.3 eV for Ag $3d_{3/2}$. The peaks are linked to Ag–O and Ag–O–Ag groups, indicating the incorporation of silver into the MOF structure. The FT-IR spectra of the U-AgMOF displayed multiple prominent peaks, suggesting the existence of diverse functional groups [26]. The wide peak range between 2700 and 3500 cm^{-1} is associated with hydroxyl groups and potentially adsorbed water. The peaks at 703–899 cm^{-1} represent the C–H bond, and the peaks at 1162 cm^{-1} and 1193 cm^{-1} correspond to the C-O group. The C=C stretching vibration occurs within the 1394–1446 cm^{-1} range. Three peaks at 1681 cm^{-1}, 1664 cm^{-1}, and 1605 cm^{-1} signify the interaction between carbonyl groups in BTC and silver ions. This reaction is essential for creating the MOF, indicating the successful coordination between the silver ions and the organic ligands in the MOF. The X-ray diffraction (XRD) pattern of the U-AgMOF shows clear peaks that correspond to individual crystalline planes [26]. Peaks at 2θ values of 39.2°, 43.88°, 65.35°, and 74.95° correspond to the (111), (200), (220), and (311) planes of a face-centered cubic crystal structure commonly found in silver nanoparticles [26].

Transmission electron microscopy (TEM) and scanning electron microscopy (SEM) analyses of the U-AgMOF nanoparticles provide important insights into their morphological and physical characteristics (Fig. 3d, e). The TEM images showed evenly distributed nanoparticles with consistent size and shape at the nanoscale, indicating a successful synthesis process. Consistency in nanoparticle morphology is essential for applications that rely on particle size and shape to determine surface area and reactivity. The SEM analysis revealed a unique surface morphology of the U-AgMOF nanoparticles, reflecting the specific crystalline structure and the silver-based framework. The surface textures play a crucial role in applications that involve surface reactions, as they directly impact how nanoparticles interact with other molecules and surfaces. Dynamic light scattering (DLS) results presented information about the size distribution of the U-AgMOF nanoparticles (Fig. 3f). The size distribution observed is a crucial parameter that impacts the physical properties, including sedimentation behavior, diffusion rates, and overall stability of nanoparticles in colloidal systems. Consistent and precise particle size distribution is crucial for maintaining reliable performance in real-world scenarios. The average particle size of the U-AgMOF was 33.6 nm, as determined by DLS. Zeta potential measurements of the U-AgMOF nanoparticles provide insight into their colloidal stability. The zeta potential's magnitude directly indicates the electrostatic interactions among suspended particles. Greater absolute values of zeta potential generally indicate increased stability, decreasing aggregation likelihood. This stability is crucial in systems where nanoparticles must stay dispersed for long periods or in changing environmental conditions [28]. The significant absolute value of − 89.24 mV for the U-AgMOF nanoparticles indicates excellent stability, which decreases their propensity to aggregate [26]. Stability is vital in systems where nanoparticles must stay dispersed for long periods or in different environmental conditions [29].

4 Two-dimensional (2D) materials hybrid nanocomposites of U-AgMOF

The integration of 2D materials, GO and $Ti_3C_2T_x$ MXene, with the U-AgMOF showcases its versatility in forming novel nanocomposites (Fig. 4a shows the schematic structure of these hybrid materials). These integrations result in materials that harness the unique properties of each component, yielding multifunctional composites with enhanced performance. U-AgMOF, in its bare form, presents a lattice framework characterized by the coordination of silver ions with organic ligands. Its integration with GO, a carbon-based material with a rich array of functional groups like carboxyl, epoxide, and hydroxyl groups, leads to the formation of a composite where U-AgMOF nanoparticles are uniformly distributed on the GO sheets [26]. This uniform distribution, as revealed by TEM images (Fig. 4b, c), indicates a strong interaction between U-AgMOF and GO, likely facilitated by π–π interactions and hydrogen bonding between the functional groups of GO and the organic ligands of U-AgMOF [30].

$Ti_3C_2T_x$ MXene, another 2D material known for its high electrical conductivity and hydrophilic nature, can also be integrated with U-AgMOF (Fig. 4d) [31]. This integration would result in a composite where the metallic nature of

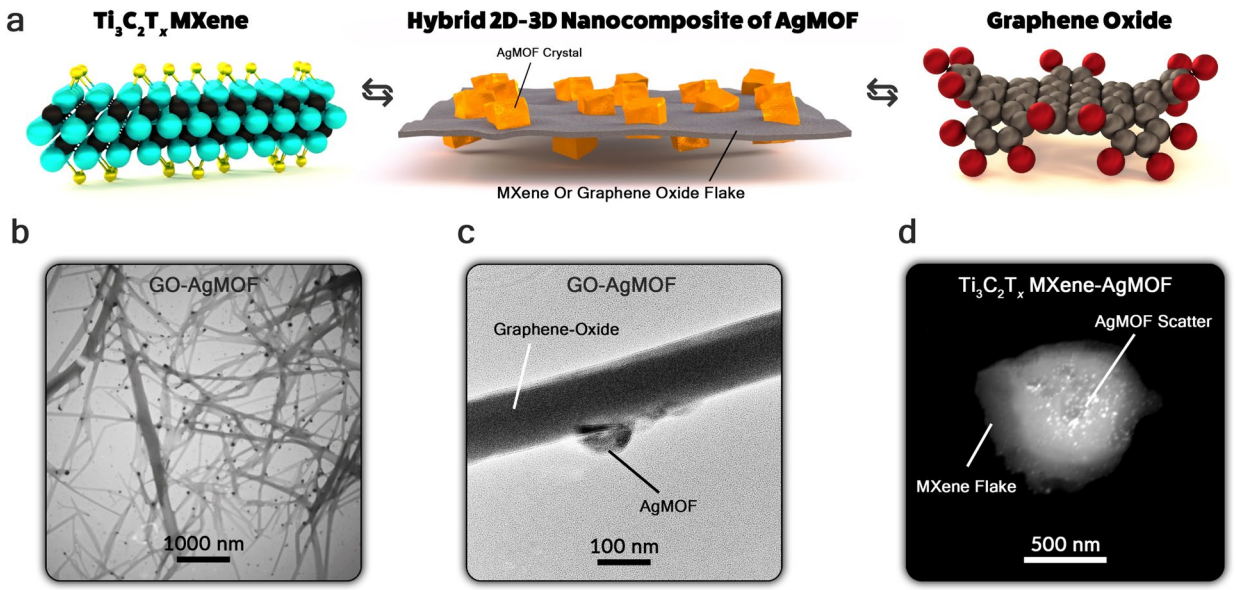

Fig. 4 The effective combination of U-AgMOF with 2D nanomaterials like GO and MXene showcases the sophisticated structural design of hybrid 2D-3D nanocomposites. **a** The layered structures of $Ti_3C_2T_x$ MXene and GO, progressing to their combined formation with U-AgMOF. TEM images in panels (**b** and **c**) the even dispersion of U-AgMOF nanoparticles on the GO sheets. **d** A $Ti_3C_2T_x$ MXene flake adorned with U-AgMOF nanoparticles indicates the possibility of improved electronic and adsorptive characteristics in these novel composite materials

MXene complements the porous structure of U-AgMOF. Such a combination could be particularly beneficial in applications requiring electrical conductivity, such as sensors or energy storage devices, while also leveraging the porosity of U-AgMOF for adsorption and catalysis applications. The integration of U-AgMOF with these materials is not just a physical mixing but a strategic combination that results in hybrid structures with improved properties. For instance, the combination with GO could lead to increased surface area and mechanical strength, making the composite suitable for environmental applications like water purification or gas adsorption. On the other hand, integrating MXene could impart electronic or photonic properties, opening up applications in electronic devices or electrocatalysis.

Moreover, the versatility of U-AgMOF extends to its ability to form composites with other materials, such as polymers, other metal oxides, or even biological molecules. Each of these combinations results in unique properties. For example, polymer integration could enhance the mechanical stability and processability of U-AgMOF, making it suitable for fabrication into films or membranes. In contrast, combining U-AgMOF with biological molecules could lead to biomedical applications like drug delivery or biosensing, where the porosity of U-AgMOF can be utilized for loading and releasing therapeutic agents. In conclusion, the integration of U-AgMOF with 2D materials like GO and MXene, and its versatility in forming various other composites, underscore its potential as a multifaceted material in advanced applications. The resulting hybrid materials not only retain the individual properties of each component but also exhibit new functionalities arising from the synergistic combination, paving the way for innovative applications in diverse fields.

5 Versatility in applications of U-AgMOF

U-AgMOF represents a pioneering class of materials demonstrating remarkable versatility across multiple fields. This section encapsulates the breadth of U-AgMOF applications, highlighting their transformative impact in areas ranging from healthcare to environmental science. U-AgMOFs are particularly noted for their potent antibacterial and anticancer properties, offering new avenues in life sciences. Additionally, their efficacy in dye adsorption marks them as valuable tools for environmental remediation. In the realm of material science, U-AgMOFs contribute significantly to the advancement of membrane technologies, enhancing properties such as hydrophilicity and antifouling capabilities in filtration systems. These diverse applications underscore the multifunctionality and potential of U-AgMOFs in addressing complex challenges in various sectors. Figure 5 schematically illustrates different

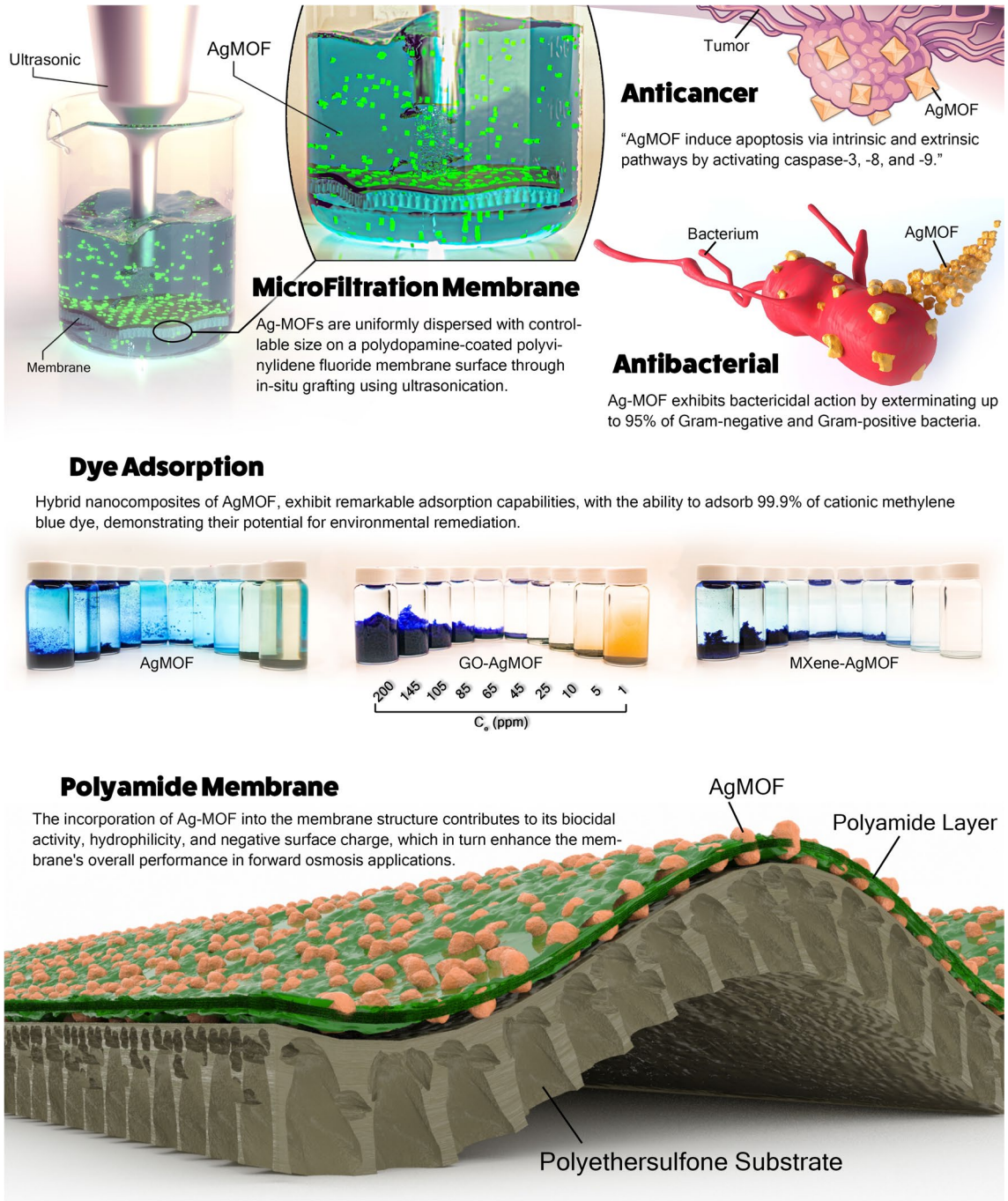

Fig. 5 Schematic illustration of U-AgMOF applications in various fields. It demonstrates its significant influence in the fields of healthcare and environmental remediation. U-AgMOFs have been observed to induce apoptosis in cancer cells via both intrinsic and extrinsic mechanisms. Additionally, they have demonstrated strong bactericidal properties, resulting in a significant reduction in bacterial growth in *E. coli* and *B. subtilis*. From an environmental perspective, U-AgMOFs demonstrate notable capabilities in adsorbing dyes, indicating their potential significance in endeavors related to water purification. The integration of U-AgMOFs into polyamide membranes in the field of material science yields sophisticated filtration systems that exhibit enhanced hydrophilicity and antifouling properties. This underscores the versatile capabilities of U-AgMOFs in diverse technological domains

applications of U-AgMOF in our previous published studies [26, 31–34].

5.1 Antibacterial applications of U-AgMOF

Firouzjaei et al. [26] reported the antibacterial properties of an U-AgMOF and GO-AgMOF, focusing on its efficacy against both Gram-negative bacteria Escherichia coli (*E. coli*) and Gram-positive bacteria Bacillus subtilis (*B. subtilis*). This comprehensive study, supported by a strong experimental approach, provides a detailed perspective on the potential of U-AgMOF as an antimicrobial agent. An essential component of the research entailed evaluating the influence of U-AgMOF on the kinetics of bacterial growth. The growth of bacteria in the presence of U-AgMOF was monitored using optical density (OD) measurements at a wavelength of 600 nm (OD600). The results indicated a concentration-dependent inhibition of bacterial growth. For instance, when *E. coli* and *B. subtilis* were exposed to 25 and 50 µg/mL concentrations of U-AgMOF for three hours, the OD600 ratios (OD-treated/OD-untreated) for *E. coli* and *B. subtilis* decreased to approximately 0.5 and 0.4, respectively. This decline signifies a substantial reduction in bacterial growth, affirming the antimicrobial potency of U-AgMOF.

Further, flow cytometry (FC) and fluorescence imaging (FI) analyses were employed to elucidate the mechanism of U-AgMOF's antibacterial action. These techniques, through the use of propidium iodide (PI) staining, allowed for the differentiation between live and dead bacterial cells. Remarkably, exposure to 100 µg/mL of U-AgMOF led to an increase in the dead cell population of *E. coli* from about 5 to 75%, indicating a significant bactericidal effect. Similarly, FI analysis showed that the proportion of dead *E. coli* cells rose from approximately 2% in untreated samples to 95% and 85% in samples treated with 100 µg/mL of GO-AgMOF and U-AgMOF, respectively. *B. subtilis* exhibited a different response to U-AgMOF treatment. The FC and FI analyses revealed that both GO-AgMOF and U-AgMOF induced a dramatic reduction in the viable cell count of *B. subtilis*. The percentage of dead *B. subtilis* cells increased from about 4% in untreated samples to around 78% and 70% for cells treated with GO-AgMOF and U-AgMOF nanoparticles, respectively. This observation suggests a distinct bacteriolytic activity of U-AgMOF against *B. subtilis*. The study proposes that the antibacterial mechanism of U-AgMOF may involve the disruption of bacterial cell membranes, leading to increased permeability and consequent cellular damage. This hypothesis is supported by the enhanced uptake of PI, a nucleic acid stain that only permeates cells with compromised membranes, in the treated bacterial populations.

While U-AgMOF has demonstrated significant antibacterial properties, a comparison with other MOFs further justifies its advantages. Other AgMOFs, for example, display considerable antibacterial activity primarily through the release of Ag + ions. However, studies have shown that the rapid release of Ag^+ from regular AgMOFs, such as in Ag-MOF composites with carbon quantum dots, can lead to a high initial antibacterial effect, but also result in cytotoxicity due to uncontrolled silver-ion release [35, 36]. For example, Travlou et al. [35] showed that Ag-MOF composites were found to degrade by about 70–80% after 24 h, affecting their long-term antibacterial efficacy. In contrast, U-AgMOF presents a more controlled release profile, as demonstrated by the sustained antibacterial activity observed against *E. coli* and *B. subtilis* in this study. Compared to zinc-based MOFs, such as ZIF-8, which also exhibit strong antibacterial properties due to zinc ion release, U-AgMOF shows a broader antibacterial spectrum. For instance, ZIF-8 demonstrated about 80% efficacy against *E. coli* after 24 h, but its antibacterial activity diminished in complex bacterial environments, such as Luria Bertani (LB) media, due to accelerated degradation [37]. In comparison, U-AgMOF maintains its antibacterial efficacy longer, with an 85–95% reduction in viable *E. coli* and *B. subtilis* cell populations under experimental conditions.

Moreover, in comparison with MOFs such as Cu/H_3BTC, which exhibited approximately 90% inhibition against *E. coli* and *Staphylococcus aureus* due to cell membrane disruption, U-AgMOF provides similar or superior antibacterial effects [38]. However, U-AgMOF has the added advantage of lower cytotoxicity, making it a more suitable candidate for long-term antimicrobial applications in medical and environmental fields.

5.2 Anticancer properties of U-AgMOF

Rezaeipour et al. [33] studied the anticancer properties of U-AgMOF. This work offers a comprehensive analysis from a biochemistry perspective, focusing on quantitative results, mechanisms, and outcomes. U-AgMOF nanoparticles were tested against SW480 colon cancer cells, and the cell viability was measured using the MTT assay. The assay results showed a dose-dependent cytotoxicity of U-AgMOF. For example, at a concentration of 12.63 µg/mL, the U-AgMOF demonstrated a significant cytotoxic impact on SW480 cells. This data indicates the potency of U-AgMOF at relatively low concentrations, which is crucial in reducing systemic toxicity in potential therapeutic applications. The study also delved into the mechanism of U-AgMOF's cytotoxicity, focusing on apoptosis induction. Flow cytometry tests were conducted using FITC-Annexin-V/PI staining to assess the apoptotic impact of U-AgMOF on cancer cells. The results revealed that at a concentration of 200 µg/mL, U-AgMOF induced a considerable increase in apoptotic cells. Specifically, the percentage of early and late apoptotic SW480 cells treated with U-AgMOF were 16.1% and 65.4%, respectively.

Furthermore, the study investigated caspase activity to understand the pathway of apoptosis induction. The caspase-3, -8, and -9 multiplex activity assay indicated a significant increase in caspase activity in cells treated with U-AgMOF. For instance, the activity of caspase-3, -8, and -9 increased 2.3-fold, 1.89-fold, and 1.70-fold, respectively, in cells treated with U-AgMOF compared to the control group. These results suggest that the anticancer activity of U-AgMOF is mediated through the intrinsic and extrinsic apoptotic pathways. Apoptotic gene expression analysis was also performed using quantitative polymerase chain reaction (qPCR). The study demonstrated an increase in the BAX/BCL2 mRNA expression ratio after treatment with U-AgMOF, indicating an enhancement in pro-apoptotic signaling pathways. The DNA fragmentation test, a hallmark of apoptosis, was conducted using Hoechst staining. The results showed a significant increase in DNA fragmentation in SW480 cells treated with U-AgMOF, indicating effective induction of apoptosis at the cellular level.

Studies on Ag-MOF derivatives, such as an organosilver(I) MOF, have shown notable anticancer activity, particularly due to the formation of silver nanoparticles. For example, Ag-MOF-derived nanoparticles exhibited IC50 values of 0.97 μM against A549 lung cancer cells, significantly outperforming the original erlotinib drug ligand [39]. However, U-AgMOF showed a different mechanism by inducing apoptosis in SW480 colon cancer cells, leading to a significant cytotoxic effect even at low concentrations, with an IC50 value of 12.63 μg/mL, highlighting its potency at lower doses compared to some Ag-MOFs. Additionally, comparisons with other MOFs, such as Zr-based MOFs like UiO-66 and UiO-67, have demonstrated their use as drug delivery systems for hydrophobic and hydrophilic anticancer drugs like paclitaxel and cisplatin. These MOFs show controlled drug release and reduced toxicity but may not match the high intrinsic anticancer activity of U-AgMOF, which directly affects cancer cell viability through both intrinsic and extrinsic apoptotic pathways [40].

Moreover, MOF-based systems that encapsulate Ag nanoparticles, such as those in a ZIF-8 framework, have shown promising anticancer effects. For instance, ZIF-8-based systems generated ultrasmall Ag nanoparticles that exhibited high-performance anticancer activity, with significant efficacy against breast cancer cells [41]. However, U-AgMOF demonstrated a more substantial apoptotic impact on SW480 cells, with apoptosis rates reaching 65.4%, compared to these frameworks, which rely on nanoparticle release and reactive oxygen species (ROS) production for their anticancer effects. This comparison illustrates that while regular AgMOF and other MOFs demonstrate strong anticancer potential, U-AgMOF's ability to induce both apoptosis and caspase activation at lower concentrations provides a more efficient and targeted approach to cancer treatment.

5.3 Dye adsorption properties of U-AgMOF

Firouzjaei et al. [31] studied the dye adsorption properties of U-AgMOF, particularly focusing on methylene blue (MB) and orange G (OG) dyes. The analysis of this paper reveals significant insights into the adsorption mechanisms and efficiencies of U-AgMOF, delineating its potential for environmental remediation. Adsorption kinetics were pivotal in understanding the interaction between U-AgMOF nanoparticles and the dyes. For MB, an adsorption efficiency exceeding 98% was achieved, with a specific mass adsorbed surpassing 390 mg/g after 14 h of exposure. In contrast, the adsorption of OG was markedly less efficient, reaching a mere 15% (specific mass adsorbed lower than 60 mg/g) under similar conditions. The substantial difference in adsorption efficiency between MB and OG highlights the influence of dye characteristics and U-AgMOF interactions in the adsorption process. The study utilized the intra-particle diffusion, pseudo-first-order, and pseudo-second-order models to describe the adsorption kinetics. The pseudo-first-order model showed the highest alignment with the experimental data, suggesting its suitability in characterizing the adsorption phenomena. The specific adsorbed mass predicted by this model ranged between 430 and 480 mg/g for MB, closely matching the experimental findings and indicating that the adsorption followed a physisorption process. Analysis of the adsorption isotherms further corroborates these findings. While the Temkin model did not satisfactorily predict the adsorption behavior, the Langmuir and Freundlich models provided a better fit. The Freundlich model, supporting multilayer adsorption, was found to be most appropriate for explaining the adsorption process, as evidenced by high R-squared values close to 1.

The adsorption mechanism was explored through the intra-particle diffusion model, which described two distinct stages for MB adsorption. Initially, there was a sharp increase in adsorption, attributed to the rapid interaction of MB with the surface of the adsorbents, followed by an equilibrium stage where most of the MB molecules were adsorbed. For OG, the data exhibited a linear trend, consistent with higher R-squared values, suggesting that the adsorption mechanism was primarily governed by intra-particle diffusion. In conclusion, this study illuminates the excellent adsorption capacity of U-AgMOF for MB, with more than 98% removal efficiency in 24 h at pH 7. This contrasts starkly with the significantly lower adsorption efficiency for OG, particularly at higher pH values. These findings underscore the efficacy and potential of U-AgMOF in dye removal applications, with a specific focus on cationic dyes like MB,

and highlight the critical role of electrostatic interactions and physisorption mechanisms in the adsorption process.

In addition to U-AgMOF's demonstrated high adsorption efficiency for MB, it is crucial to compare its performance with regular AgMOF and other MOFs. Other AgMOF composites, such as Ag-MOF combined with carbon quantum dots, have been shown to exhibit strong adsorption properties. For example, Ag-MOF@AA hybrid systems achieved an MB adsorption capacity of 768 mg/g, indicating effective removal of MB from solutions [42]. This performance is comparable to the adsorption capacity of U-AgMOF, which achieved a 98% removal rate with an adsorption capacity exceeding 390 mg/g. When comparing U-AgMOF to other MOFs, such as UiO-66, the difference becomes more apparent in terms of adsorption efficiency for different dyes. UiO-66, a Zr-based MOF, demonstrated a maximum adsorption capacity of 454 mg/g for methyl orange (MO) and 370 mg/g for MB [43]. While this is competitive, U-AgMOF's ability to achieve over 98% removal efficiency for MB in 24 h, combined with its unique structural properties and electrostatic interactions, gives it an edge in applications involving cationic dyes. Additionally, the Langmuir adsorption model fits well for U-AgMOF, similar to other MOFs like UiO-66.

5.4 U-AgMOF application in polyamide membranes

Firouzjaei et al. [32] studied the fabrication of U-AgMOF incorporated thin-film nanocomposite (TFN) membranes, an innovative approach that significantly enhances their properties and performance. The U-AgMOF membranes were fabricated using a two-step interfacial polymerization technique, involving the deposition of U-AgMOF nanoparticles onto a polysulfone support, followed by the formation of a polyamide active layer. The process began with the immersion of the polysulfone support into an aqueous solution containing U-AgMOF nanoparticles. This step allowed for the uniform distribution and adherence of U-AgMOF nanoparticles onto the polysulfone substrate. Subsequently, the coated support was immersed in an organic solution containing trimesoyl chloride (TMC), a common organic monomer used in interfacial polymerization. The interaction between the aqueous phase (containing U-AgMOF) and the organic phase (containing TMC) at the interface resulted in the formation of a thin polyamide layer, effectively embedding the U-AgMOF nanoparticles within the PA matrix. This fabrication approach yielded TFN membranes with distinct characteristics, combining the advantageous properties of U-AgMOF, such as enhanced hydrophilicity and antibacterial activity, with the robustness and selectivity of traditional PA membranes.

The successful integration of U-AgMOF into the membrane structure was confirmed through various characterization techniques, including SEM, atomic force microscopy (AFM), and XPS. The resulting U-AgMOF TFN membranes demonstrated significant improvements in surface roughness, hydrophilicity, and antifouling performance compared to traditional TFC membranes. The surface roughness, as measured by AFM, showed that the U-AgMOF TFN membrane had a mean roughness (Sa) of 386 ± 6 nm and an RMS roughness (Sq) of 442 ± 19 nm, which was significantly higher than that of the TFC membrane. The increased surface roughness is attributed to the embedment of the U-AgMOF nanoparticles in the top surface of the membrane. Contact angle measurements further revealed the enhanced hydrophilicity of the U-AgMOF TFN membranes. The GO-AgMOF TFN membrane exhibited the lowest contact angle of $54° \pm 3$, indicating a high level of surface hydrophilicity, which is beneficial for antifouling applications. XPS analyses provided insights into the elemental compositions and bonding characteristics of the membranes. Peaks at 285.0 eV in the C 1s spectra were observed across all membrane types, while the U-AgMOF TFN and GO-AgMOF TFN membranes showed distinctive features in their Ag 3d spectra, confirming the presence of U-AgMOF. Performance metrics such as water and solute permeability coefficients indicated that the U-AgMOF TFN membrane had a water permeability of 1.70 ± 0.16 L/(m2·h·bar) and a solute permeability of 0.19 ± 0.02 L/(m2·h), demonstrating enhanced water permeability with acceptable solute barrier properties.

Other Ag-MOF-based membranes, such as those utilizing Ag-MOF nanorods, have demonstrated improved antibacterial properties, with reductions in bacterial attachment by over 92% when low amounts of Ag-MOF nanorods were incorporated into the polyamide layer [44]. However, U-AgMOF membranes show enhanced long-term antifouling stability, with higher water flux recovery rates of over 95% and minimal biofilm formation when exposed to *E. coli* and *B. subtilis*. In comparison with other MOFs, such as those incorporating GO into polyamide membranes, the performance differences become clearer. GO-modified membranes increased water permeability and antifouling capabilities but faced limitations in salt rejection performance, particularly in forward osmosis applications [45]. U-AgMOF, on the other hand, retains superior water permeability (1.70 L/m^2·h·bar) and solute rejection performance (0.19 L/m2·h), while also offering better biofilm resistance due to its silver-ion controlled release, which limits bacterial growth over extended filtration cycles.

Furthermore, compared to membranes incorporating standard hydrophilic additives, such as polyamide (PA-6) membranes, which showed a tenfold increase in permeability but reduced antifouling properties [46], U-AgMOF membranes provide a balanced performance of both high

permeability and superior long-term antifouling performance without compromising selectivity. This positions U-AgMOF as a superior material for advanced membrane technologies.

5.5 Application of U-AgMOF in microfiltration membranes

Zolghadr et al. [34] explored the fabrication of U-AgMOF grafted on polyvinylidene fluoride (PVDF) microfiltration membranes, focusing on enhanced antibacterial and antifouling properties. The fabrication process of these U-AgMOF modified membranes is a critical aspect that underpins their unique properties and applications. The U-AgMOF nanoparticles were synthesized and grafted onto the membrane surface using a sonochemical process, recognized for its energy efficiency and environmental friendliness. Sonochemistry, which involves ultrasonic methods, is advantageous due to its ability to synthesize materials at lower energy inputs and ambient conditions. This method was selected over conventional electric heating, microwave heating, and other methods due to its efficiency and the quality of the nanoparticles produced. In the conventional method of U-AgMOF synthesis, nanoparticles are pre-synthesized and then applied to a substrate. However, a significant limitation of this approach is that the U-AgMOF nanoparticles do not robustly react with the substrate and can be easily washed away during the rinsing process. This issue was observed when U-AgMOF nanoparticles were applied to a non-coated PVDF substrate, where they could not efficiently bind and were quickly removed during washing.

To overcome these challenges, the researchers employed a different strategy involving the in situ grafting of U-AgMOFs onto the membrane substrate. This approach ensured a stronger interaction between the U-AgMOF nanoparticles and the membrane surface, leading to a more stable and effective functionalization. The resulting U-AgMOF functionalized PVDF membranes demonstrated significant improvements in surface properties compared to traditional membranes. These enhancements included increased surface roughness and hydrophilicity, which contributed to the membranes' improved antibacterial and antifouling properties. The study's findings highlight the potential of U-AgMOF functionalized membranes in applications where the suppression of biofilm development and bacterial inactivation are crucial, especially in water treatment processes. The innovative fabrication process of these membranes represents a significant advancement in membrane technology, offering new opportunities for the development of efficient and sustainable water treatment solutions.

Table 1 The environmental impacts of 1 kg U-AgMOF synthesis in the laboratory scale

Impact category	Unit	1 kg of U-AgMOF
Acidification	kg SO2 eq	37.1
Carcinogenics	CTUh	7.39E-04
Ecotoxicity	CTUe	326885.6
Eutrophication	kg N eq	30.9
Fossil fuel depletion	MJ surplus	29786.0
Global warming	kg CO2 eq	9770.1
Noncarcinogenics	CTUh	3.89E-03
Ozone depletion	kg CFC-11 eq	7.18E-04
Respiratory effects	kg PM2.5 eq	8.3
Smog	kg O3 eq	531.8

Compared to other AgMOFs, U-AgMOF provides improved long-term stability. For instance, standard Ag-MOF/PVDF membranes reduce *E. coli* growth by approximately 91%, but the antibacterial efficacy decreases significantly after 48 h due to rapid silver-ion release, leading to a diminished effect over time [47]. In contrast, U-AgMOF exhibits a controlled release of silver ions, maintaining over 85% antibacterial efficacy for up to 7 days, providing more sustained protection against bacterial adhesion and biofilm formation.

In comparison with other MOFs, such as GO-CNC composite membranes, which achieve a flux recovery ratio of approximately 90%, U-AgMOF membranes demonstrate similar or slightly better flux recovery ratio, maintaining around 85–90% even after extended filtration cycles. GO-CNC-modified membranes show a decrease in flux recovery after prolonged use due to their susceptibility to chemical degradation, whereas U-AgMOF maintains mechanical integrity and superior antifouling performance for up to 14 days [48]. Additionally, when compared to membranes incorporating additives like zwitterionic SiO_2 nanoparticles, which exhibit high initial water flux recovery of 95%, but limited antibacterial properties, U-AgMOF membranes offer balanced performance. U-AgMOF not only maintains a high flux recovery (85–90%) but also achieves a 70–80% reduction in bacterial adhesion, ensuring a longer-lasting antifouling capability [49].

Table 2 The energy demand of 1 kg U-AgMOF synthesis in the laboratory scale

Impact category	Unit	1 kg of U-AgMOF
Fossil	MJ	239928.5
Biomass	MJ	1.3
Nuclear	MJ	23203.4
Biomass	MJ	1526.6
Water	MJ	3171.4
Wind, Solar, Geothermal	MJ	1217.3

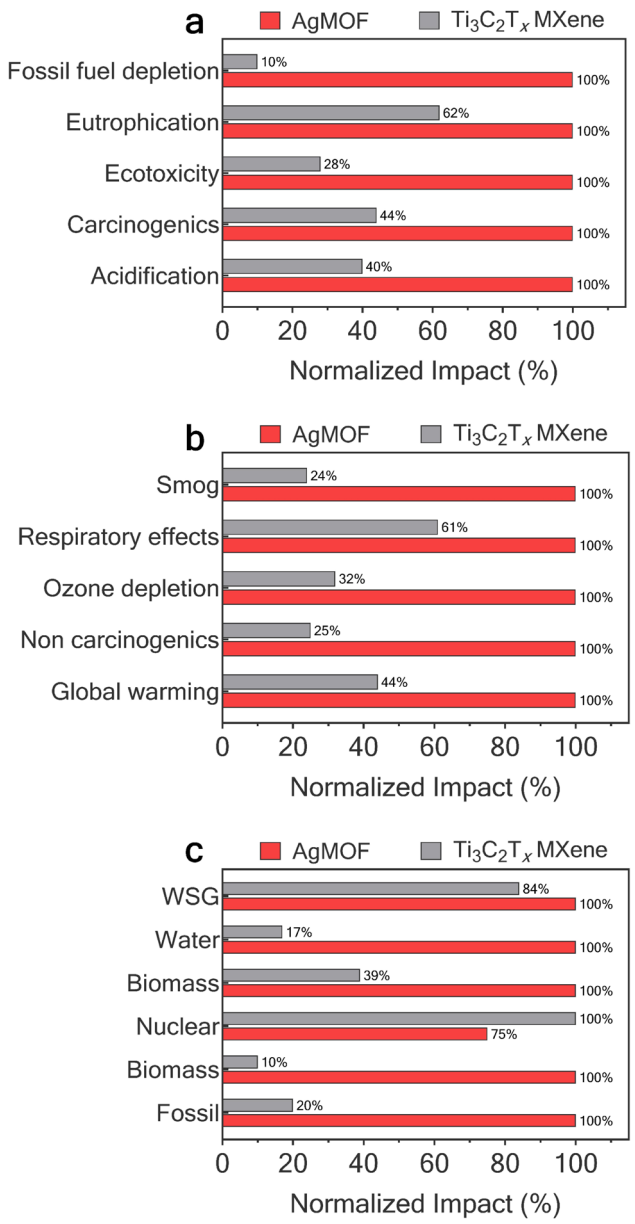

Fig. 6 Comparative life cycle assessment (LCA) impact of 1 kg of U-AgMOF versus $Ti_3C_2T_x$ MXene across various environmental categories (**a**, **b**) and cumulative energy demand (CED) categories. The data illustrate U-AgMOF's higher relative environmental impact in all categories, with significant differences noted in categories such as acidification, ecotoxicity, and fossil fuel depletion. The CED comparison highlights U-AgMOF's substantial demand for fossil, biomass, and nonrenewable energy sources compared to MXene, emphasizing the need for improved sustainability in U-AgMOF production processes

6 Life cycles assessment of U-AgMOF and industrial status of MOFs

LCA is a critical tool in evaluating the environmental footprint of novel materials such as U-AgMOFs, and conducting this analysis is paramount in the era of sustainable development. This research is pioneering in executing a comprehensive LCA for U-AgMOFs, a study not previously documented in scientific literature. Tables 1, 2 represent the environmental impacts and energy demands for the fabrication of 1 kg U-AgMOF on a laboratory scale, respectively. To better understand the LCA results of the U-AgMOF fabrication, the U-AgMOF LCA results are compared to our previous study's [50] material, $Ti_3C_2T_x$ MXene (Fig. 6). This shows that the laboratory-scale fabrication of 1 kg of U-AgMOF has higher environmental impact across all categories than $Ti_3C_2T_x$ MXene. The energy demand and environmental impact are notably higher for the production of U-AgMOF, as indicated by the 100% impact across all categories, which starkly contrasts with the lower percentages for $Ti_3C_2T_x$ MXene. For instance, the acidification potential of U-AgMOF is more than double that of MXene, indicating that the production of U-AgMOF may contribute more substantially to the potential for acid rain. Similarly, the data suggest that the production of U-AgMOF is more demanding in terms of cumulative energy demand (CED), with a complete reliance on fossil, biomass, and renewable sources, compared to $Ti_3C_2T_x$ MXene which shows a more diversified and lower reliance on these energy sources. The higher ecological and health impact categories for U-AgMOF warrant attention, including carcinogenic and noncarcinogenic effects, ecotoxicity, and respiratory effects. The ecotoxicity category, for instance, demonstrates that U-AgMOF's production is potentially more harmful to aquatic life than $Ti_3C_2T_x$ MXene in this scale. This could be due to the chemicals and solvents used in synthesizing U-AgMOF, which may have higher toxicity profiles.

The grouped LCA data for U-AgMOF fabrication reveals that the majority of environmental impacts are due to chemical use, with significant contributions also from electricity, and to a much lesser extent, waste generation (Fig. 7). Chemicals dominate the impact in nearly all categories, particularly in fossil fuel depletion (95%), indicating that the synthesis of U-AgMOF is heavily reliant on chemical processes that are possibly energy-intensive and may involve nonrenewable resource inputs. Electricity usage also plays a considerable role, especially in categories like eutrophication (30.2%) and respiratory effects (29.6%), suggesting that energy consumption during production is a critical factor in these environmental impacts. Waste generation contributes minimally across all categories, which could indicate either an efficient use of materials with little by-product formation or effective waste management strategies. Overall, this analysis underscores the need to optimize chemical inputs and energy consumption in U-AgMOF production to reduce its environmental footprint.

The detailed LCA data disaggregated by chemical inputs presents an insightful perspective on the environmental burdens associated with the fabrication of 1 kg of U-AgMOF.

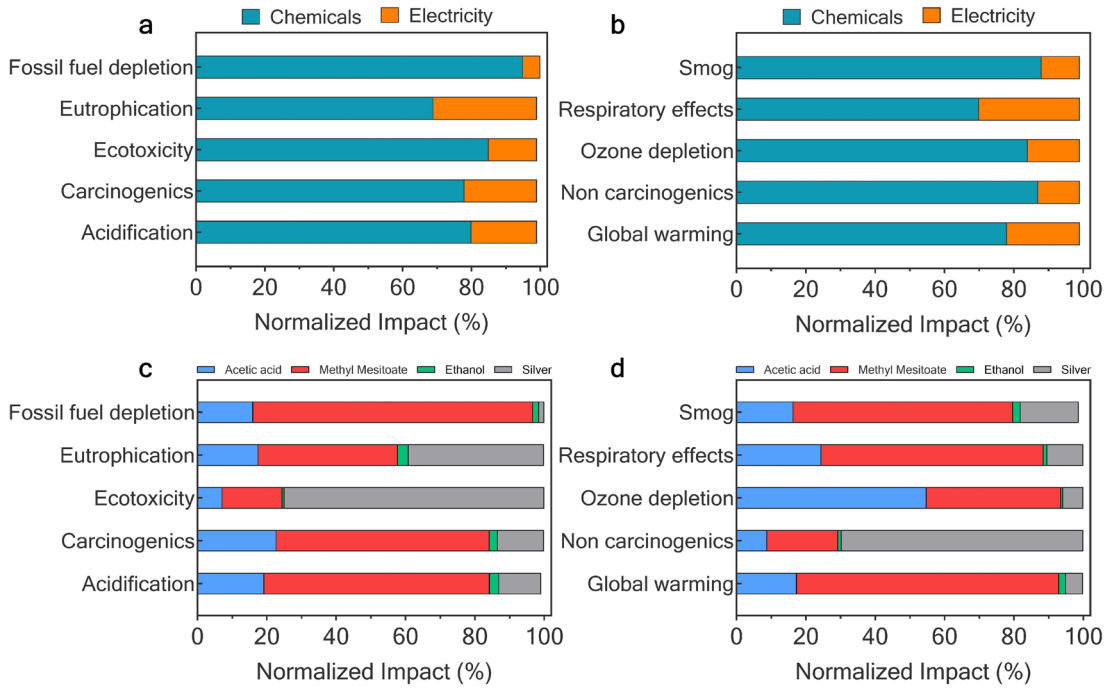

Fig. 7 Breakdown of normalized environmental impacts by process inputs for the production of 1 kg of U-AgMOF. **a**, **b** display the impacts categorized by chemicals and electricity, with chemicals being the predominant contributor in categories like fossil fuel depletion and ecotoxicity. **c**, **d** further dissect the chemical contributions, highlighting the dominant influence of methyl mesitoate across most impact categories, particularly in fossil fuel depletion and global warming, while acetic acid and silver show a substantial contribution to ozone depletion and ecotoxicity, respectively

Methyl mesitoate, the principal chemical component, accounts for a significant majority of impacts across most categories, notably 80.7% in fossil fuel depletion and 75.6% in global warming, indicating its substantial contribution to nonrenewable resource use and greenhouse gas emissions. Acetic acid and ethanol show more moderate impacts, while silver, despite its low percentage, notably leads in ecotoxicity with 74.9%, reflecting its high environmental persistence and potential for bioaccumulation. These insights are crucial for targeting specific stages in the production process for sustainability improvements, such as the substitution of chemicals with lower environmental impacts or the optimization of silver usage. The negligible impact of deionized (DI) water suggests an efficient use of water in the process. This analysis underscores the need for environmental optimization in U-AgMOF production, particularly focusing on the chemicals used.

LCA is indispensable for gauging the environmental implications of manufacturing and deploying materials such as U-AgMOFs, especially when considering the scale-up for industrial applications. It is important to identify and mitigate potential environmental impacts early in the development and commercialization phases. LCA enables researchers and industry leaders to make informed decisions that align with sustainable development goals. It identifies hotspots of environmental stress, guides eco-design principles, and supports policy and strategic decisions for materials that are likely to be produced and used on a large scale. Conducting LCA in the industrialization phase of a material can help in optimizing the production process to minimize environmental impact, meet regulatory requirements, and enhance the market competitiveness of the material by demonstrating a commitment to sustainability. The LCA of U-AgMOFs has illuminated the predominant environmental impact stemming from specific chemical precursors used in its synthesis, particularly methyl mesitoate. To mitigate this, future research could explore alternative organic linkers that are less resource-intensive and generate fewer emissions during their lifecycle. Substituting methyl mesitoate with more environmentally benign alternatives could significantly lower the fossil fuel depletion and global warming impact categories. Moreover, the utilization of silver, a major contributor to ecotoxicity, calls for a reassessment of the quantity used, recycling of silver waste, or replacement with less toxic metals where possible without compromising the functionality of MOFs. Energy consumption patterns also warrant optimization, particularly through the implementation of renewable energy sources in production processes, which could address the impacts associated with electricity use. These focused strategies are not only pivotal for improving

the environmental profile of U-AgMOFs but also essential for their responsible scale-up to industrial levels.

6.1 Industrial marketing of metal–organic frameworks

In the burgeoning field of advanced materials, MOFs represent a significant leap forward due to their unique properties and potential applications [51]. Industries are increasingly focusing on the development and application of MOFs, leveraging their high surface area, tunable pore sizes, and versatile chemistry for various innovative uses. This section of the manuscript delves into the landscape of MOF-based industries, illustrating their pioneering efforts and the potential pathways to commercialization and industrial impact.

BASF, a global chemical company, has taken the lead in the production of MOFs at an industrial scale [52]. With a robust portfolio of MOF materials, BASF has tackled applications such as CO_2 capture and storage, showcasing their commitment to environmental sustainability. Their collaboration with Svante Technologies, for instance, has led to the scale-up of a novel MOF material tailored for efficient carbon capture, demonstrating the potential to reduce industrial carbon footprints significantly. These technologies have demonstrated the versatility of MOFs by diversifying their applications, such as in postharvest management of fresh produce. Their collaboration with the agricultural sector to extend the shelf life of fruits and vegetables exemplifies the role of MOFs in sectors beyond traditional chemical applications. Such innovations reflect the potential of MOFs to penetrate various market segments, offering solutions to real-world challenges. NuMat Technologies, originating from academic research, illustrates the successful transition from laboratory to market [53]. Their focus on integrating MOFs into systems for storing and handling hazardous gases is a testament to the commercial viability and industrial demand for MOFs in high-tech applications, including the microelectronics industry.

The MOF industry has seen a considerable increase in market size and is projected to grow significantly [54]. The global MOFs market, which stood at USD 351.89 million in 2022, is forecasted to reach USD 1395.88 million by 2029, with a compound annual growth rate (CAGR) of 20.94% during the forecast period [54]. The industry is marked by the presence of key players like BASF, MOFapps, Strem Chemicals, MOF Technologies, and Framergy. These companies are engaged in various applications of MOFs ranging from gas storage to catalysis. The growth in the market is driven by the versatility of MOFs and their increasing integration into industrial applications.

The exploration of these industries reveals a promising trend in the adoption of MOFs for commercial applications, laying the groundwork for further industrialization. The narrative of MOF-based industries is marked by innovation, collaboration, and a strong orientation toward sustainability. These industrial efforts are pivotal in driving the scale-up of MOF production, signifying a forward trajectory in the implementation of these materials across diverse sectors. As MOF technologies continue to evolve, it is imperative to support their trajectory from niche to mainstream applications. This will involve addressing challenges in scalability, cost, and integration into existing industrial processes. With ongoing research and development, the day when MOFs become a staple in various industries may not be far off, marking a new era of material science where functionality meets sustainability.

7 Future direction of U-AgMOF in membrane research

The future direction of MOF research within the membrane field should pivot toward scaling up and in situ fabrication techniques, as demonstrated by recent advances [55–58]. These methodologies enable the production of large-area, ultrathin MOF membranes with enhanced durability and applicability in industrial processes, particularly for gas separation and water treatment. By focusing on scalable, efficient fabrication processes, U-AgMOF membrane technology can overcome previous limitations, offering novel solutions for environmental and industrial challenges. This shift toward practical, large-scale application underscores the significant potential of U-AgMOF membranes in sustainable technology development.

Qiao et al. [56] introduced a novel step-nucleation in situ self-repair strategy for fabricating large-area (2400 cm2), ultrathin, and rollable MOF membranes. This method enables the production of MOF membranes on a flexible polymer membrane support, combining a polyvinyl alcohol (PVA)–metal-ion layer with a pure metal-ion layer. The latter serves as the main nucleation site for MOF growth, while the PVA–metal-ion layer acts as a slow-release metal-ion source, aiding in defect repair. This approach resulted in the successful creation of a 4800 cm2 spiral-wound membrane module, demonstrating the feasibility of applying large-area MOF membranes in practical applications. The process emphasizes the importance of MOF membranes for gas separation, highlighting the potential for industrial application by overcoming previous limitations in MOF membrane scalability and durability.

8 LCA methodology

This study assesses the energy and environmental impacts of producing 1 kg of U-AgMOF. The synthesis process is derived from the content presented in Sect. 3 of this paper. The inventory file for the fabrication process is provided as

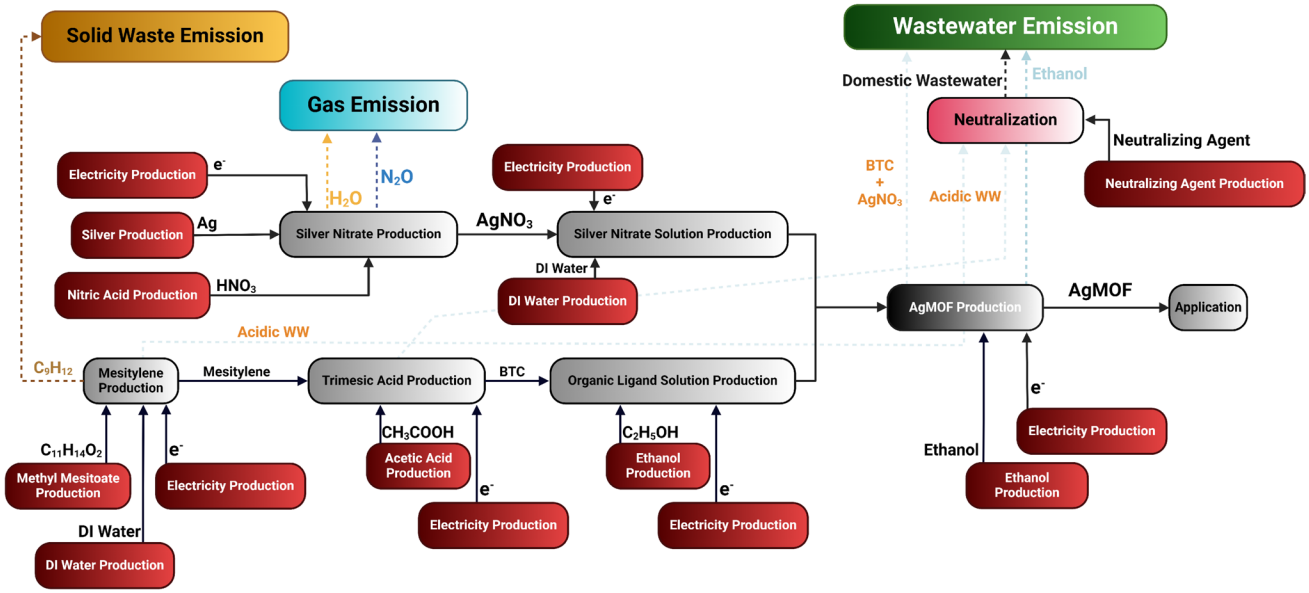

Fig. 8 The cradle-to-gate life cycle assessment (LCA) boundaries used to analyze the entire life cycle of producing 1 kg of U-AgMOF

supplementary material to this paper. Figure 8 displays the cradle-to-gate system boundaries used in the LCA methodology for synthesizing U-AgMOF. The computations were executed utilizing the ecoinvent database and the OpenLCA software. The LCA of $Ti_3C_2T_x$ MXene is obtained from our previous research [50]. The comprehensive details regarding the LCA of MXene are available in our prior research [50]. The study was set for Alabama, USA. LCA methodologies were utilized to obtain the products' CED, while the Tool for the Reduction and Assessment of Chemical and other Environmental Impacts (TRACI 2.1) was employed to determine the associated environmental impacts of the functional units. It was understood that selecting from these impact categories was a normative decision influenced by the individual values of each user. The United States Environmental Protection Agency (US EPA) initiated a taxonomy analysis to identify potential consequences and impact categories that should be comprehensively considered during the initial selection process. Additional details regarding the LCA methods, comprehensive definitions of each impact category, and a complete inventory list of all calculations can be found in the Supporting Information.

9 Declaration of Artificial Intelligence (AI) Usage and Authorship Contributions

The authors declare that artificial intelligence (AI) assistance was utilized during the preparation of this manuscript. The AI was employed solely for language refinement, grammar correction, and formatting suggestions based on the authors' input. All scientific content, ideas, analyses, interpretations, and conclusions were solely conceived, verified, and approved by the authors. Additionally, no AI was used in the design or depiction of figures; all visual elements were created entirely by the first author. The use of AI was under strict human oversight, and its contributions were aligned with the ethical guidelines of academic writing and publishing.

Supplementary Information The online version contains supplementary material available at https://doi.org/10.1007/s41127-024-00083-9.

Acknowledgements This research benefitted greatly from funding provided by USDA TAT-RWTS 00-69526. This paper has not been formally reviewed by USDA, and the views expressed in this document are solely those of the authors and do not necessarily reflect those of USDA. USDA does not endorse any products or commercial services mentioned in this publication. USDA had no role in the study design, data collection, analysis, publication decision, or manuscript preparation.

Author contributions M.D.F. wrote the manuscript, curated the data, ran the life cycle assessment, initiated the paper, and supervised the project. A.A.S., A.R., and F.A.A. helped review and edit the manuscript and methodologies. M.E. assisted with manuscript revision, methodology, funding acquisition, and project supervision.

Data availability No datasets were generated or analyzed during the current study.

Declarations

Competing interests The authors declare no competing interests.

References

1. Tomic E (1965) Thermal stability of coordination polymers. J Appl Polym Sci 9(11):3745–3752
2. Czaja AU, Trukhan N, Müller U (2009) Industrial applications of metal–organic frameworks. Chem Soc Rev 38(5):1284–1293
3. Biondi C, Bonamico M, Torelli L, Vaciago A (1965) On the structure and water content of copper(II) tricyanomethanide. J Chem Soc Chem Commun. https://doi.org/10.1039/c19650000191
4. Hoskins BF, Robson R (1990) Design and construction of a new class of scaffolding-like materials comprising infinite polymeric frameworks of 3D-linked molecular rods. A reappraisal of the zinc cyanide and cadmium cyanide structures and the synthesis and structure of the diamond-related frameworks [N (CH3) 4][CuIZnII (CN) 4] and CuI [4, 4', 4'', 4'''-tetracyanotetraphenylmethane] BF4. xC6H5NO2. J Am Chem Soc 112(4):1546–1554
5. Li H, Eddaoudi M, O'Keeffe M, Yaghi OM (1999) Design and synthesis of an exceptionally stable and highly porous metal-organic framework. Nature 402(6759):276–279
6. Dybtsev DN, Chun H, Yoon SH, Kim D, Kim K (2004) Microporous manganese formate: a simple metal−organic porous material with high framework stability and highly selective gas sorption properties. J Am Chem Soc 126(1):32–33. https://doi.org/10.1021/ja038678c
7. Zhang X, Lin R-B, Wang J, Wang B, Liang B, Yildirim T, Zhang J, Zhou W, Chen B (2020) Optimization of the pore structures of MOFs for record high hydrogen volumetric working capacity. Adv Mater 32(17):1907995. https://doi.org/10.1002/adma.201907995
8. Furukawa H, Cordova KE, O'Keeffe M, Yaghi OM (2013) The chemistry and applications of metal-organic frameworks. Science 341(6149):1230444
9. Alhamami M, Doan H, Cheng C-H (2014) A review on breathing behaviors of metal-organic-frameworks (MOFs) for gas adsorption. Materials 7(4):3198–3250
10. Cai G, Yan P, Zhang L, Zhou H-C, Jiang H-L (2021) Metal-organic framework-based hierarchically porous materials: synthesis and applications. Chem Rev 121(20):12278–12326. https://doi.org/10.1021/acs.chemrev.1c00243
11. Seetharaj R, Vandana P, Arya P, Mathew S (2019) Dependence of solvents, pH, molar ratio and temperature in tuning metal organic framework architecture. Arab J Chem 12(3):295–315
12. Azbell TJ, Pitt TA, Bollmeyer MM, Cong C, Lancaster KM, Milner PJ (2023) Ionothermal synthesis of metal-organic frameworks using low-melting metal salt precursors. Angew Chem 135(17):e202218252
13. Biswal D, Kusalik PG (2017) Probing molecular mechanisms of self-assembly in metal-organic frameworks. ACS Nano 11(1):258–268. https://doi.org/10.1021/acsnano.6b05444
14. Lollar CT, Qin J-S, Pang J, Yuan S, Becker B, Zhou H-C (2018) Interior decoration of stable metal–organic frameworks. Langmuir 34(46):13795–13807
15. Sánchez-Sánchez M, Getachew N, Díaz K, Díaz-García M, Chebude Y, Díaz I (2015) Synthesis of metal–organic frameworks in water at room temperature: salts as linker sources. Green Chem 17(3):1500–1509
16. Li Y, Yang RT (2007) Gas adsorption and storage in metal—organic framework MOF-177. Langmuir 23(26):12937–12944
17. Furukawa H, Miller MA, Yaghi OM (2007) Independent verification of the saturation hydrogen uptake in MOF-177 and establishment of a benchmark for hydrogen adsorption in metal–organic frameworks. J Mater Chem 17(30):3197–3204
18. Yang K, Sun Q, Xue F, Lin D (2011) Adsorption of volatile organic compounds by metal–organic frameworks MIL-101: influence of molecular size and shape. J Hazard Mater 195:124–131. https://doi.org/10.1016/j.jhazmat.2011.08.020
19. Bhattacharjee S, Chen C, Ahn W-S (2014) Chromium terephthalate metal–organic framework MIL-101: synthesis, functionalization, and applications for adsorption and catalysis. RSC Adv 4(94):52500–52525
20. Sotnik SA, Gavrilenko KS, Lytvynenko AS, Kolotilov SV (2015) Catalytic activity of copper(II) benzenetricarboxylate (HKUST-1) in reactions of aromatic aldehydes condensation with nitromethane: kinetic and diffusion study. Inorg Chimica Acta 426:119–125. https://doi.org/10.1016/j.ica.2014.11.018
21. Liu Y, Zhang T, Wu W, Jiang S, Zhang H, Li B (2015) Water-mediated promotion of direct oxidation of benzene over the metal–organic framework HKUST-1. RSC Adv 5(69):56020–56027. https://doi.org/10.1039/C5RA05595D
22. Li C, Tang H, Fang Y, Xiao Z, Wang K, Wu X, Niu H, Zhu C, Zhou H-C (2018) Bottom-up assembly of a highly efficient metal-organic framework for cooperative catalysis. Inorg Chem 57(21):13912–13919. https://doi.org/10.1021/acs.inorgchem.8b02434
23. Babu DJ, He G, Hao J, Vahdat MT, Schouwink PA, Mensi M, Agrawal KV (2019) Restricting lattice flexibility in polycrystalline metal–organic framework membranes for carbon capture. Adv Mater 31(28):1900855
24. Vendite AC, Soares TA, Coutinho K (2022) The effect of surface composition on the selective capture of atmospheric CO2 by ZIF nanoparticles: the case of ZIF-8. J Chem Inf Model 62(24):6530–6543. https://doi.org/10.1021/acs.jcim.2c00579
25. Wang Y, Lin W, Yu S, Huang X, Lang X, He Q, Gao L, Zhu H, Chen J (2021) A biocompatible Zr-based metal-organic framework UiO-66-PDC as an oral drug carrier for pH-response release. J Solid State Chem 293:121805. https://doi.org/10.1016/j.jssc.2020.121805
26. Firouzjaei MD, Shamsabadi AA, Sharifian Gh M, Rahimpour A, Soroush M (2018) A novel nanocomposite with superior antibacterial activity: a silver-based metal organic framework embellished with graphene oxide. Adv Mater Interfaces 5(11):1701365. https://doi.org/10.1002/admi.201701365
27. Mardani M, Siahtiri S, Besati M, Baghani M, Baniassadi M, Nejad AM (2024) Microencapsulation of natural products using spray drying; an overview. J Microencapsul 41:649
28. Selmani A, Ulm L, Kasemets K, Kurvet I, Erceg I, Barbir R, Pem B, Santini P, Marion ID, Vinković T, Krivohlavek A, Sikirić MD, Kahru A, Vinković Vrček I (2020) Stability and toxicity of differently coated selenium nanoparticles under model environmental exposure settings. Chemosphere 250:126265. https://doi.org/10.1016/j.chemosphere.2020.126265
29. Phan HT, Haes AJ (2019) What does nanoparticle stability mean? J Phys Chem C 123(27):16495–16507. https://doi.org/10.1021/acs.jpcc.9b00913
30. Siahtiri S, Sahraei AA, Mokarizadeh AH, Baghani M, Bodaghi M, Baniassadi M (2023) Influence of curing agents molecular structures on interfacial characteristics of graphene/epoxy nanocomposites: a molecular dynamics framework. Macromol Mater Eng 308(8):2300030
31. Dadashi Firouzjaei M, Zolghadr E, Arabi Shamsabadi A, Sadrzadeh M, Rahimpour A, Akbari Afkhami F, Wujcik EK, Elliott M (2023) Clean water recycling through adsorption via heterogeneous nanocomposites: silver-based metal-organic framework embellished with graphene oxide and MXene. Case Stud Chem Environ Eng 7:100296. https://doi.org/10.1016/j.cscee.2023.100296
32. Firouzjaei MD, Shamsabadi AA, Aktij SA, Seyedpour SF, Sharifian Gh M, Rahimpour A, Esfahani MR, Ulbricht M, Soroush M (2018) Exploiting synergetic effects of graphene oxide and a silver-based metal-organic framework to enhance antifouling and anti-biofouling properties of thin-film nanocomposite

membranes. ACS Appl Mater Interfaces 10(49):42967–42978. https://doi.org/10.1021/acsami.8b12714
33. Rezaeipour Y, Zolghadr E, Alizadeh P, Sadri G, Wujcik EK, Afkhami FA, Elliott M, Dadashi Firouzjaei M (2022) The anticancer properties of metal-organic frameworks and their heterogeneous nanocomposites. Biomater Adv 139:213013. https://doi.org/10.1016/j.bioadv.2022.213013
34. Zolghadr E, Dadashi Firouzjaei M, Aghapour Aktij S, Aghaei A, Wujcik EK, Sadrzadeh M, Rahimpour A, Afkhami FA, LeClair P, Elliott M (2022) An ultrasonic-assisted rapid approach for sustainable fabrication of antibacterial and anti-biofouling membranes via metal-organic frameworks. Mater Today Chem 26:101044. https://doi.org/10.1016/j.mtchem.2022.101044
35. Travlou NA, Algarra M, Alcoholado C, Cifuentes-Rueda M, Labella AM, Lázaro-Martínez JM, Rodríguez-Castellón E, Bandosz TJ (2018) Carbon quantum dot surface-chemistry-dependent ag release governs the high antibacterial activity of Ag-metal–organic framework composites. ACS Appl Bio Mater 1(3):693–707. https://doi.org/10.1021/acsabm.8b00166
36. Wu Y, Zhang L, Zhou Y, Zhang L, Li Y, Liu Q, Hu J, Yang J (2019) Light-induced ZnO/Ag/rGO bactericidal photocatalyst with synergistic effect of sustained release of silver ions and enhanced reactive oxygen species. Chin J Catal 40(5):691–702. https://doi.org/10.1016/S1872-2067(18)63193-6
37. Taheri M, Ashok D, Sen T, Enge TG, Verma NK, Tricoli A, Lowe A, Nisbet DR, Tsuzuki T (2021) Stability of ZIF-8 nanopowders in bacterial culture media and its implication for antibacterial properties. Chem Eng J 413:127511. https://doi.org/10.1016/j.cej.2020.127511
38. Shams S, Ahmad W, Memon AH, Shams S, Wei Y, Yuan Q, Liang H (2020) Cu/H3BTC MOF as a potential antibacterial therapeutic agent against staphylococcus aureus and *Escherichia coli*. New J Chem 44(41):17671–17678. https://doi.org/10.1039/D0NJ04120C
39. Song C-Y, Zhang J-Y, Qiu Y, Jin H-P, Zhang H-M, Liu S, Liu H, Qiu H-B, Gao G-G (2019) Value-added anticancer reactivity of sub-5 nm Ag-drug nanoparticles derived from organosilver(I) MOF. Sci China Chem 62(3):347–354. https://doi.org/10.1007/s11426-018-9376-7
40. Filippousi M, Turner S, Leus K, Siafaka PI, Tseligka ED, Vandichel M, Nanaki SG, Vizirianakis IS, Bikiaris DN, Van Der Voort P, Van Tendeloo G (2016) Biocompatible Zr-based nanoscale MOFs coated with modified poly(ε-caprolactone) as anticancer drug carriers. Int J Pharm 509(1):208–218. https://doi.org/10.1016/j.ijpharm.2016.05.048
41. Li Y, Gao Z, Zhang Y, Chen F, An P, Wu H, You C, Sun B (2021) MOF-shielded and glucose-responsive ultrasmall silver nano-factory for highly-efficient anticancer and antibacterial therapy. Chem Eng J 416:127610. https://doi.org/10.1016/j.cej.2020.127610
42. Ribeiro SC, de Lima HHC, Kupfer VL, da Silva CTP, Veregue FR, Radovanovic E, Guilherme MR, Rinaldi AW (2019) Synthesis of a superabsorbent hybrid hydrogel with excellent mechanical properties: water transport and methylene blue absorption profiles. J Mol Liq 294:111553. https://doi.org/10.1016/j.molliq.2019.111553
43. Ahmadijokani F, Mohammadkhani R, Ahmadipouya S, Shokrgozar A, Rezakazemi M, Molavi H, Aminabhavi TM, Arjmand M (2020) Superior chemical stability of UiO-66 metal-organic frameworks (MOFs) for selective dye adsorption. Chem Eng J 399:125346. https://doi.org/10.1016/j.cej.2020.125346
44. Seyedpour SF, Dadashi Firouzjaei M, Rahimpour A, Zolghadr E, Arabi Shamsabadi A, Das P, Akbari Afkhami F, Sadrzadeh M, Tiraferri A, Elliott M (2020) Toward sustainable tackling of biofouling implications and improved performance of TFC FO membranes modified by Ag-MOF nanorods. ACS Appl Mater Interfaces 12(34):38285–38298. https://doi.org/10.1021/acsami.0c13029
45. Izadmehr N, Mansourpanah Y, Ulbricht M, Rahimpour A, Omidkhah MR (2020) TETA-anchored graphene oxide enhanced polyamide thin film nanofiltration membrane for water purification; performance and antifouling properties. J Environ Manag 276:111299. https://doi.org/10.1016/j.jenvman.2020.111299
46. Shockravi A, Vatanpour V, Najjar Z, Bahadori S, Javadi A (2017) A new high performance polyamide as an effective additive for modification of antifouling properties and morphology of asymmetric PES blend ultrafiltration membranes. Microporous Mesoporous Mater 246:24–36. https://doi.org/10.1016/j.micromeso.2017.03.013
47. Abdul-Majeed MA (2018) Preparation and characterization of AgNp/PVDF composite ultrafiltration membrane. J Eng 24(7):50–63. https://doi.org/10.31026/j.eng.2018.07.04
48. Lv J, Zhang G, Zhang H, Yang F (2018) Graphene oxide-cellulose nanocrystal (GO-CNC) composite functionalized PVDF membrane with improved antifouling performance in MBR: behavior and mechanism. Chem Eng J 352:765–773. https://doi.org/10.1016/j.cej.2018.07.088
49. Zhu J, Zhao X, He C (2015) Zwitterionic SiO2 nanoparticles as novel additives to improve the antifouling properties of PVDF membranes. RSC Adv 5(66):53653–53659. https://doi.org/10.1039/C5RA05571G
50. Dadashi Firouzjaei M, Nemani SK, Sadrzadeh M, Wujcik EK, Elliott M, Anasori B (2023) Life-cycle assessment of Ti3C2Tx MXene synthesis. Adv Mater 35(31):2300422. https://doi.org/10.1002/adma.202300422
51. Zhang H, Nai J, Yu L, Lou XW (2017) Metal-organic-framework-based materials as platforms for renewable energy and environmental applications. Joule 1(1):77–107. https://doi.org/10.1016/j.joule.2017.08.008
52. Hoffmann K (2023) BASF becomes first company to successfully produce metal-organic frameworks on a commercial scale for carbon capture. https://www.basf.com/global/en/media/news-releases/2023/10/p-23-327
53. Benyo S (2024) Numat announces launch of SENTINEL™ filtration platform, revolutionizing chemical protection technology for 21st century threats. https://www.numat.com/news/numat-announces-launch-of-sentinel/
54. Metal Organic Frameworks Market - By product (Aluminum, Copper, Iron, Zinc, Magnesium), By Synthetic market (Hydro thermal, Microwave, ultrasonic, mechanochemical, electrochemical), By Application (catalyst, carbon capture) - Global Forecast to 2032 (2023)
55. Pejman M, Dadashi Firouzjaei M, Aghapour Aktij S, Das P, Zolghadr E, Jafarian H, Arabi Shamsabadi A, Elliott M, Sadrzadeh M, Sangermano M, Rahimpour A, Tiraferri A (2020) In situ Ag-MOF growth on pre-grafted zwitterions imparts outstanding antifouling properties to forward osmosis membranes. ACS Appl Mater Interfaces 12(32):36287–36300. https://doi.org/10.1021/acsami.0c12141
56. Qiao Z, Liang Y, Zhang Z, Mei D, Wang Z, Guiver MD, Zhong C (2020) Ultrathin low-crystallinity MOF membranes fabricated by interface layer polarization induction. Adv Mater 32(34):2002165. https://doi.org/10.1002/adma.202002165
57. He S, Zhu B, Jiang X, Han G, Li S, Lau CH, Wu Y, Zhang Y, Shao L (2022) Symbiosis-inspired de novo synthesis of ultrahigh MOF growth mixed matrix membranes for sustainable carbon capture. Proc Natl Acad Sci 119(1):e2114964119. https://doi.org/10.1073/pnas.2114964119
58. Yao B, Hussain S, Ye Z, Peng X (2023) Electrodeposited MOFs membrane with in situ incorporation of charged molecules for

osmotic energy harvesting. Small 19(18):2207559. https://doi.org/10.1002/smll.202207559

Terms and Conditions

Springer Nature journal content, brought to you courtesy of Springer Nature Customer Service Center GmbH (“Springer Nature”).
Springer Nature supports a reasonable amount of sharing of research papers by authors, subscribers and authorised users (“Users”), for small-scale personal, non-commercial use provided that all copyright, trade and service marks and other proprietary notices are maintained. By accessing, sharing, receiving or otherwise using the Springer Nature journal content you agree to these terms of use (“Terms”). For these purposes, Springer Nature considers academic use (by researchers and students) to be non-commercial.
These Terms are supplementary and will apply in addition to any applicable website terms and conditions, a relevant site licence or a personal subscription. These Terms will prevail over any conflict or ambiguity with regards to the relevant terms, a site licence or a personal subscription (to the extent of the conflict or ambiguity only). For Creative Commons-licensed articles, the terms of the Creative Commons license used will apply.
We collect and use personal data to provide access to the Springer Nature journal content. We may also use these personal data internally within ResearchGate and Springer Nature and as agreed share it, in an anonymised way, for purposes of tracking, analysis and reporting. We will not otherwise disclose your personal data outside the ResearchGate or the Springer Nature group of companies unless we have your permission as detailed in the Privacy Policy.
While Users may use the Springer Nature journal content for small scale, personal non-commercial use, it is important to note that Users may not:

1. use such content for the purpose of providing other users with access on a regular or large scale basis or as a means to circumvent access control;
2. use such content where to do so would be considered a criminal or statutory offence in any jurisdiction, or gives rise to civil liability, or is otherwise unlawful;
3. falsely or misleadingly imply or suggest endorsement, approval , sponsorship, or association unless explicitly agreed to by Springer Nature in writing;
4. use bots or other automated methods to access the content or redirect messages
5. override any security feature or exclusionary protocol; or
6. share the content in order to create substitute for Springer Nature products or services or a systematic database of Springer Nature journal content.

In line with the restriction against commercial use, Springer Nature does not permit the creation of a product or service that creates revenue, royalties, rent or income from our content or its inclusion as part of a paid for service or for other commercial gain. Springer Nature journal content cannot be used for inter-library loans and librarians may not upload Springer Nature journal content on a large scale into their, or any other, institutional repository.
These terms of use are reviewed regularly and may be amended at any time. Springer Nature is not obligated to publish any information or content on this website and may remove it or features or functionality at our sole discretion, at any time with or without notice. Springer Nature may revoke this licence to you at any time and remove access to any copies of the Springer Nature journal content which have been saved.
To the fullest extent permitted by law, Springer Nature makes no warranties, representations or guarantees to Users, either express or implied with respect to the Springer nature journal content and all parties disclaim and waive any implied warranties or warranties imposed by law, including merchantability or fitness for any particular purpose.
Please note that these rights do not automatically extend to content, data or other material published by Springer Nature that may be licensed from third parties.
If you would like to use or distribute our Springer Nature journal content to a wider audience or on a regular basis or in any other manner not expressly permitted by these Terms, please contact Springer Nature at

onlineservice@springernature.com